Organic Electronics 13 (2012) 1229–1236

Contents lists available at SciVerse ScienceDirect

Organic Electronics

journal homepage: www.elsevier.com/locate/orgel

Phase dependence of hole mobilities in dibenzo-tetrathiafulvalene crystal: A first-principles study

Guangjun Nan [a,*], Zesheng Li [a,b,c,*]

[a] Institute of Theoretical and Simulational Chemistry, Academy of Fundamental and Interdisciplinary Sciences, Harbin Institute of Technology, 150080 Harbin, People's Republic of China
[b] School of Chemistry, Beijing Institute of Technology, 100081 Beijing, People's Republic of China
[c] Key Laboratory of Cluster Science of Ministry of Education, Beijing Institute of Technology, 100081 Beijing, People's Republic of China

ARTICLE INFO

Article history:
Received 6 January 2012
Received in revised form 26 March 2012
Accepted 27 March 2012
Available online 17 April 2012

Keywords:
Organic semiconductor
Dibenzo-tetrathiafulvalene
Marcus charge transfer rate
Charge mobility
Density functional theory

ABSTRACT

The organic semiconductor dibenzo-tetrathiafulvalene (DBTTF) has presented different polymorphs in solid packing, but the structure–property relationship is little clarified in the literature which is important for the design of high-performance organic semiconductors. In this study, the charge transport in DBTTF crystals for the α phase and β phase is investigated from the first-principles calculations and the Marcus charge transfer theory. The one-, two- and three-dimensional mobilities are obtained simultaneously from a set of identical trajectories with an improved random walk technique. It is found that the α-phase crystal presents a smaller three-dimensional mobility than that in the β-phase crystal although the mobility is much large along the *c* axis in the α-phase crystal. This is attributed to that the electronic couplings are mainly confined within the *c* axis for the α-DBTTF while the electronic couplings are more uniform in the three-dimensional space for the β-DBTTF which thus provides more transport pathways for the charge transport. As a result, the β-DBTTF may have a larger potential for practical applications in organic electronics.

1. Introduction

A growing interest in organic field-effect transistors (OFETs) has merged in past years due to their potential applications to low-cost, large-area, and flexible devices [1–3]. The carrier mobility, which is an important parameter for estimating the performance of OFETs, has been improved significantly over the past two decades [4]. The highest OFETs mobilities have been reported for vacuum-deposited crystalline films or single crystals of low-molecular weight species and, in particular, pentacene-based transistors have received special attention [5–7]. However, the pentacene is not suitable for low-cost integrated circuit technology because of its very low solubility in organic solvents. Therefore, a large number of molecular materials have been designed in recent years to achieve relatively high carrier mobilities in OFETs [8].

Tetrathiafulvalene (TTF) derivatives have been shown to be one kind of prospective organic materials for practical applications in OFETs [9] because of the following two advantages: (i) they are obtained in simple synthetic procedures to allow for the easy attainment of substituted or modified TTF molecules; and (ii) their processability is advantageous because of their good solubility in common organic solvents. Furthermore, the mobilities in TTF derivatives have been comparable to those of conventional amorphous silicon FETs [10]. For example, Mas-Torrent et al. have reported high mobilities of 1.4 $cm^2 V^{-1} s^{-1}$ using dithiophene-TTF in a single-crystal OFET processed from solutions [11]. Naraso et al. have achieved a mobility of

* Corresponding authors. Address: Institute of Theoretical and Simulational Chemistry, Academy of Fundamental and Interdisciplinary Sciences, Harbin Institute of Technology, 150080 Harbin, People's Republic of China (G. Nan).
E-mail addresses: gjnan@hit.edu.cn (G. Nan), zeshengli@hit.edu.cn (Z. Li).

1566-1199/$ - see front matter © 2012 Elsevier B.V. All rights reserved.
http://dx.doi.org/10.1016/j.orgel.2012.03.033

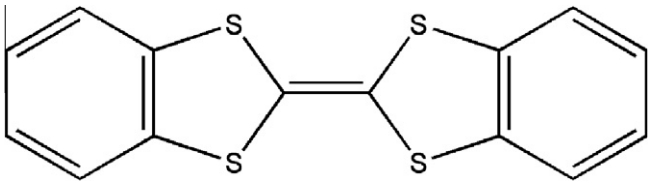

Fig. 1. Molecular structure of dibenzo-tetrathiafulvalene (DBTTF).

0.42 $cm^2 V^{-1} s^{-1}$ in an evaporated-film OFET using naphthalene-fused TTF [12]. Takahashi et al. have even performed a field-effect mobility exceeding 10 $cm^2 V^{-1} s^{-1}$ in a single-crystal OFET of hexamethylene-TTF [13]. Among the TTF-based transistors, dibenzo-TTF (DBTTF) (see Fig. 1) is a well investigated material and high mobility values, 1.0 $cm^2 V^{-1} s^{-1}$ for a single crystal and 0.55 $cm^2 V^{-1} s^{-1}$ for a thin film, have been reported [14,15]. It is noted that the crystal structure of DBTTF in Ref. [14,15] corresponds to the α-phase crystal structure in Ref. [16] where different polymorphic crystal structures of DBTTF have been exhibited. Recently, one more different herringbone phase has been obtained from sublimation for DBTTF [17], which is similar to the β-phase crystal structure in Ref. [16]. It can be observed that the α-phase crystal structure of DBTTF has a layer-by-layer packing of planar π-conjugated molecules while the β-phase crystal structure present a non-layered three-dimensional (3D) stack of the planar π-conjugated molecules [16]. The molecular packing is much different for the two crystal structures. It is now widely recognized that the mobility of OFETs is determined primarily by the molecular packing motifs that are responsible for intermolecular π–π overlaps within the channel layers [18,19] such as for pentacene [20] and rubrene [5]. However, a packing motif of non-layered 3D structure also presents much large mobilities such as for the hexamethylene-TTF [13]. Therefore, it is attractive to clarify the structure–property relationships of the α- and β-DBTTF for better understanding the carrier transport in OFETs.

The paper is arranged as follows: In Section 2, the theoretic methodology is described to calculate the charge transfer rates and to simulate the charge mobility for the α-phase and β-phase crystal structures of DBTTF. In Section 3, the numerical results and discussion are displayed. The conclusion is drawn in Section 4.

2. Theoretic methodology

2.1. Charge transfer rate

In almost all π-conjugated organic materials, the molecular scale charge transport at room temperature occurs via a thermally activated hopping type mechanism [21–24] since dynamical structural disorder strongly localizes the charge at high temperature [25,26] and invalidates the band type mechanism [27]. To describe such an incoherent hopping mechanism, the semiclassical Marcus theory is widely used in the literature [28]:

$$W = \frac{V^2}{\hbar}\left(\frac{\pi}{\lambda k_B T}\right)^{1/2} \exp\left(-\frac{\lambda}{4k_B T}\right), \tag{1}$$

where V is the transfer integral (electronic coupling) between the donor and acceptor, λ is the reorganization energy, k_B is the Boltzmann constant and T is the temperature.

The reorganization energy mainly includes the structural modification of the molecules and the surrounding mediums due to polarization effects, upon going from the neutral to the charged state and vice versa. Since the nuclear polarization contribution is expected to be significantly smaller than the intramolecular contribution [29], the present paper only considers the reorganization energy from the intramolecular structural modification which is the sum of two relaxation energy terms [30,31]:

$$\lambda = \lambda^{(1)} + \lambda^{(2)}. \tag{2}$$

For hole transport, the term $\lambda^{(1)}$ is the difference between the energies of the neutral molecule in its optimized geometry and in the optimized cationic geometry, and the term $\lambda^{(2)}$ is the difference between the energies of the cationic molecule in its optimized geometry and in the optimized neutral geometry, as shown in Fig. 2. The λ terms are evaluated in two ways: (i) directly from the adiabatic potential-energy surfaces of the neutral and cationic states [32–34] and (ii) from the normal-mode analysis through DUSHIN program [35] which provides the partition of the total relaxation energy into the contributions from each vibrational mode:

$$\lambda = \sum_i \lambda_i = \sum_i \hbar\omega_i S_i, \tag{3}$$

$$\lambda_i = \frac{k_i}{2}\Delta Q_i^2. \tag{4}$$

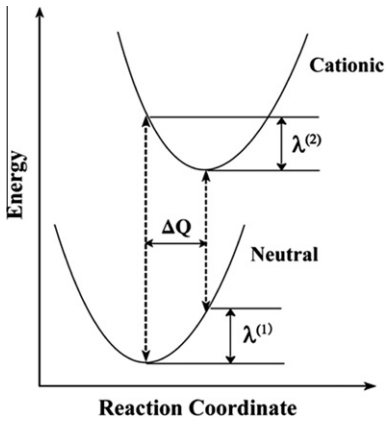

Fig. 2. Sketch of the potential energy surfaces for the neutral and cationic states, showing the vertical transitions (dashed lines), the normal mode displacement (ΔQ) and the relaxation energies ($\lambda^{(1)}$ and $\lambda^{(2)}$).

Here, the summations run over all vibrational normal modes. ΔQ_i represents the displacement along the normal mode (NM) i between the equilibrium geometries of the neutral and cationic molecules in Fig. 2, S_i denotes the Huang–Rhys factor measuring charge-phonon coupling strength, k_i and ω_i represent the corresponding force constant and vibrational frequency. In this study, the reorganization energies from the AP and NM methods are performed using the density functional theory (DFT) with the B3LYP functional and 6–31 + G** basis set from the Gaussian 03 program package [36].

The transfer integrals are usually evaluated for the nearest-neighbor molecules [37], so the single crystal structure of α- and β-DBTTF in Fig. 3 is used to generate all possible intermolecular hopping pathways. Various computational techniques have been developed to obtain the intermolecular electronic couplings [25,38–46], among which the site energy correction (SEC) method [45] has been shown to be reliable [47] and is used here to calculate the transfer integrals. For hole transport, the highest occupied molecular orbitals (HOMOs) of two isolated neutral monomers are used to construct charge localized states. The Kohn–Sham equations are then used to construct the orbitals of the dimer which are the linear combinations of the molecular orbitals of both monomers. Since the monomer orbitals are nonorthogonal, an orthonormal basis set is obtained by means of Löwdin's symmetric transformation. The transfer integral V is finally expressed as:

$$V = \frac{h_{12} - \frac{1}{2}(e_1 + e_2)S_{12}}{1 - S_{12}^2}. \tag{5}$$

Here, $e_i = \langle \Phi_i | H | \Phi_i \rangle$ $(i = 1, 2)$, $h_{12} = \langle \Phi_1 | H | \Phi_2 \rangle$, and $S_{12} = \langle \Phi_1 | S | \Phi_2 \rangle$, where Φ_1 and Φ_2 are the HOMOs of the two monomers in the dimer, H and S are the dimer Hamiltonian and the overlap matrix, respectively. In this study, the transfer integrals are evaluated at the DFT level using PW91PW91 functional and a b-31G* basis set with the Gaussian 03 program package [36]. After the reorganization energies and transfer integrals have been obtained from the above description, the charge transfer rates can be calculated with Eq. (1).

2.2. Charge mobility from random walk simulations

Given the charge transfer rates, the charge mobility is often evaluated by assuming a Brownian motion of the charge carriers in the absence of applied electric fields and using the Einstein relation [48,49]:

$$\mu = \frac{e}{k_B T} D, \tag{6}$$

where e is the electron charge, k_B is the Boltzmann constant, T is the temperature, and D is the diffusion coefficient which is defined as the ratio between the mean-square displacement (MSD) r^2 and the diffusion time t:

$$D = \frac{1}{2n} \lim_{t \to \infty} \frac{r(t)^2}{t}. \tag{7}$$

Here, n represents the transport dimension of carriers in organic materials. Experiments have shown that the charge transport in OFETs is mainly confined within the first few layers of the organic semiconductors/insulator interface [4,50,51], so the carrier is often believed to transport in 2D molecular layers which are parallel to the organic semiconductors/insulator interface [26,52] and the mobilities are obtained with $n = 2$ in Eq. (7). However, it has been noted recently that the inter-layer interactions may have an obvious influence on the charge transport in the 2D transport layer when the inter-layer interactions are large enough [53], so the mobility should be simulated from the 3D pathways with $n = 3$ in Eq. (7) for such case. Furthermore, the angular resolution anisotropic charge

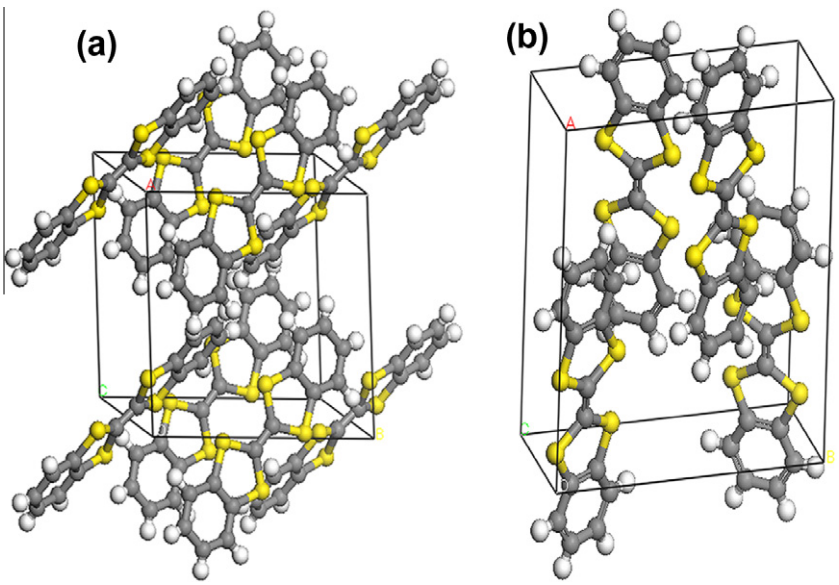

Fig. 3. Crystal structures of DBTTF: (a) the unit cell of the α phase; (b) the unit cell of the β phase.

transport has been performed in single-crystal OFETs [5,54–56], which corresponds to the carrier mobilities with $n = 1$ in Eq. (7) along various orientation angles from a theoretic viewpoint. Therefore, comparing the mobilities of different dimensions from theoretic simulation can promote the understanding of the charge transport in organic materials. To perform this goal, one molecule from the crystal structure is randomly chosen as the initial charge center. The nearest-neighbor molecules around the center molecule in 3D space are selected to construct the transport pathways. The hopping rates for the charge at the central molecule to all its neighbors are calculated with Eq. (1), so the hopping probability for the charge to the ith neighbor is $p_i = W_i/\sum_j W_j$ where the summation in the denominator runs over all the pathways in the 3D space. Then a random number r uniformly distributed between 0 and 1, is generated to determine the transport pathway for each hopping. If $\sum_{i=1}^{k-1} p_i < r \leqslant \sum_{i=1}^{k} p_i$, the charge is assumed to propagate along the kth pathway. After determining the next position for the charge carrier, the simulation time is incremented by $1/\sum_j W_j$ [57] and the hopping distance is taken to be the molecular center-center distance. The simulation continues until the total simulation time is achieved. Such simulations are repeated to get thousands of independent charge diffusion trajectories until the MSD reaches an approximately linear function of the simulation time. The diffusion coefficient for the 3D transport can be then obtained from Eq. (7) with $n = 3$. To obtain the 2D diffusion coefficient, the transport plane in which the charge mobilities are required is chosen and the angle γ between the plane and the transport distance from the initial charge center to the final position can be known, so the transport distance in the transport plane is projected from the 3D transport distance as $r\cos(\gamma)$. Then the 2D diffusion coefficient is written as:

$$D = \frac{1}{2n}\lim_{t\to\infty}\frac{r(t)^2\cos^2(\gamma)}{t}, \tag{8}$$

with $n = 2$. To further perform the angular resolution anisotropic diffusion coefficient, the transport plane is used as the reference and Φ is assumed to the orientation angle of transport channel relative to the reference axis, so the 1D transport distance in the plane is projected from the 3D transport distance as $r\cos(\gamma)\cos(\Phi)$. Thus, the anisotropic diffusion coefficient in the reference plane is expressed as:

$$D = \frac{1}{2n}\lim_{t\to\infty}\frac{r(t)^2\cos^2(\gamma)\cos^2(\Phi)}{t}, \tag{9}$$

with $n = 1$. The carrier mobilities for 3D, 2D and 1D transport can be finally evaluated from Eq. (6) with Eqs. (7)–(9), respectively. From the above description, it can be seen that the carrier mobilities for different dimensions are obtained from a set of identical trajectories.

3. Results and discussion

Previous calculations have shown that the reorganization energies from the AP and NM methods are close to each other if the basis set is large enough [40,59], so the comparison of the reorganization energies from both methods can be used to judge whether the basis set is proper. For the present DBTTF, the reorganization energy for holes is calculated as 243.7 meV and 244.5 meV from the AP and NM methods, respectively. The reorganization energies from both methods are very close. This indicates that the calculated reorganization energy is reliable with the present basis set.

To better understand the electronic couplings, it is necessary to discuss the differences between the crystal structures of DBTTF in the α and β phases [16]. For the α phase in Fig. 3(a), the crystal structure is monoclinic and has two centrosymmetric molecules per unit cell. The molecular stack forms a herringbone structure in the *b*–*c* plane with the π–π overlap between consecutive molecules along the *c* axis. As a result, the molecules form the heading-to-tail packing along the *a* axis when one side of all the molecules is denoted as heading and the other side is denoted as tail along the long axis of molecules. For the β phase in Fig. 3(b), the crystal has a monoclinic unit cell with four molecules. While the herringbone motif is also shown in the *b*–*c* plane, there is not π–π overlap any more between consecutive molecules in the stacks along the *c* axis. The adjacent molecules along the *b* axis have large displacements along the long molecular axis, which leads to a zig-zag chain along the *b* axis, so a packing motif of non-layered 3D stack is observed in the β phase. Based on the α- and β-phase crystal structures, fig. 4 presents 14 nearest-neighbor dimers which are used to construct the transport pathways. The corresponding intermolecular center-to-center distances and the transfer integrals are collected in Table. 1. It can be seen that there are the largest electronic couplings for the pathways 1 and 4 which corresponds to the *c* axis in the α-phase crystal structure. This is due to that the π–π overlap of the adjacent molecules can lead to much strong intermolecular electronic couplings [37]. Meanwhile, it is noted that the electronic couplings of the dimers in different molecular layers are much smaller than those in the molecular monolayers, which is attributed to that there is little molecular orbital overlap for the heading-to-tail stacks along the *a* axis. However, the case is different for the β-phase crystal structure that the transfer integrals are close to each other for the pathways 1–6, 9 and 10 which present the non-layered 3D stacks. Thus the electronic couplings are more uniform in the 3D space for the β-phase crystal structure than those for the α-phase crystal structure where the electronic couplings are mainly confined within the *c* axis.

The charge transfer rates for each pathway are evaluated with Eq. (1) using the reorganization energy from the AP method and the transfer integrals in table 1. Then the MSDs for $n = 1, 2, 3$ are obtained from the random walk simulation technique. In this study, 5000 random walk trajectories are performed to achieve an approximately linear relationship between the MSD and the simulation time. The MSDs for the 3D space are shown in Fig. 5 as a function of simulation time. Since the MSDs for 2D and 1D transport are different in different planes and axes, respectively, fig. 5 also presents the MSDs for the largest 2D and 1D transport. For the α phase, it can be seen that the MSDs in the 3D space and 2D plane are

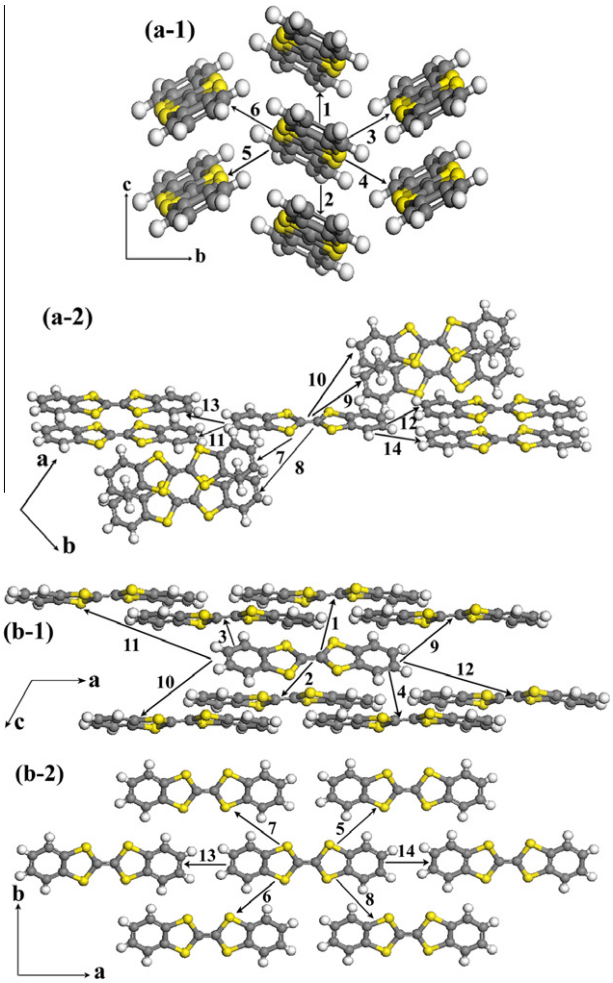

Fig. 4. The nearest-neighbor hopping pathways in DBTTF crystals: (a-1) and (a-2) for the α phase; (b-1) and (b-2) for the β phase.

Table 1
Intermolecular center-to-center distance *d* (in angstrom) and hole transfer integral *V* (in meV) of the pathways in Fig. 4 for the α-phase and β-phase DBTTF crystals.

Pathways	α phase		β phase	
	d	*V*	*d*	*V*
1	3.95	47.81	4.99	-24.58
2	3.95	47.81	4.99	-24.58
3	7.55	4.84	7.69	8.75
4	7.55	4.84	7.69	8.75
5	7.55	4.84	9.53	5.36
6	7.55	4.84	9.53	5.36
7	11.44	-0.57	9.53	0.99
8	11.44	-0.57	9.53	0.97
9	11.44	-0.57	10.20	15.20
10	11.44	-0.57	10.20	15.20
11	14.62	2.65	14.48	0.47
12	14.62	2.65	14.48	0.47
13	15.15	0.29	15.15	-1.17
14	15.15	0.29	15.15	-1.17

much close to each other, which shows that there is little probability for the charge to hop between different molecular layers and the charge transport mainly occurs in the *b*–*c* plane. The 1D MSD along the *c* axis is slightly smaller than the 2D MSD, so the charge transport in the *b*–*c* plane mainly occurs along the *c* axis. However, the case is different for the β phase that the MSD decreases obviously from the 3D space to the 2D plane and from the 2D plane to the 1D axis, respectively. This shows that there are obvious charge transports along any direction in the 3D space. To better understand the charge transport, the carrier mobilities are calculated from Eq. (6) for 3D, 2D and 1D transport. Table 2 shows that the mobility in the *a*–*b* plane is much smaller than the mobilities in the *b*–*c* and *a*–*c* planes for the α phase. To distinguish the contribution of the 2D mobilities from various transport channels, the angular resolution anisotropic mobilities are shown in Fig. 6 for the α phase. It can be seen that the mobilities are much small along any direction except the direction of the *c* axis which presents much large electronic couplings, so the large mobilities in the *b*–*c* and *a*–*c* planes mainly come from the contribution of the carrier transport along the *c* axis. This is consistent with the 1D transport character of the α phase from theoretic prediction [60] and is close to the mobility from experiment [61]. The small 2D mobility

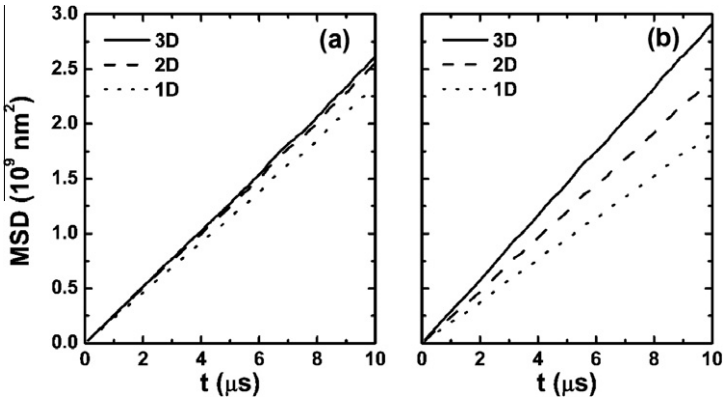

Fig. 5. The MSDs versus simulation time from average over 5000 random walk trajectories for the charge transport in 3D space, 2D plane and 1D axis: (a) for the α phase; (b) for the β phase. Since the MSDs for 2D and 1D transport are different in different planes and axes, respectively, the largest MSDs for the 2D and 1D transport are shown here, respectively. For the α phase, the 2D MSD is for the *b*–*c* plane while the 1D MSD is for the *c* axis; for the β phase, the 2D MSD is for the *a*–*c* plane while the 1D MSD is for the axis which has an angle of 140° with the reference axis *c* shown in Fig. 7(c).

Table 2
Hole mobilities (in cm^2/Vs) of the 3D space and 2D planes with the reorganization energy from the AP method for the α-phase and β-phase DBTTF crystals.

	α phase	β phase
3D space	0.166	0.189
a–*b* plane	0.026	0.156
b–*c* plane	0.244	0.181
a–*c* plane	0.231	0.233

in the *a*–*b* plane is due to the poor charge transport along any direction in the plane. However, the 2D carrier mobilities in Table 2 are close to each other in each plane for the β-phase crystal structure. This is attributed to that the more uniform electronic couplings are present in the 3D space, so a relatively balanced charge transport is observed along any direction in each plane, which can be seen from the angular resolution anisotropic mobilities in Fig. 7. As a result, the 3D mobility of the α phase is smaller than that of the β phase. Therefore, it is concluded that the uniform electronic couplings in the β-phase crystal are helpful to promote the charge transport in the 3D space although the 1D charge transport along any direction is smaller than that along the *c* axis in the α-phase crystal. It is generally accepted that the OFET mobilities are usually large for the crystal structures with the layer-by-layer packing such as for pentacene [6] and rubrene [5] because there are much large intermolecular π–π overlaps in the molecular monolayers which can lead to strong electronic couplings. The present calculations show that the non-layered 3D stacks are also advisable to perform large OFET mobilities if intermolecular π–π overlaps are decreased to a certain extent along some pathways in the molecular layers and instead the electronic couplings are increased for the adjacent molecular layers. Recently, a mobility exceeding $10\,cm^2\,V^{-1}\,s^{-1}$ has been achieved in the single-crystal OFET of hexamethylene-TTF [13] which has a non-layered 3D stacks. It is interesting to note that the mobility of hexamethylene-TTF is much larger than the mobilities of the other TTF derivatives such as dithiophene-TTF [11] and dinaphtho-TTF [12] where the layer-by-layer packing is present. The variations of the mobilities in these organic materials can be understood from the present study although the further work is still required.

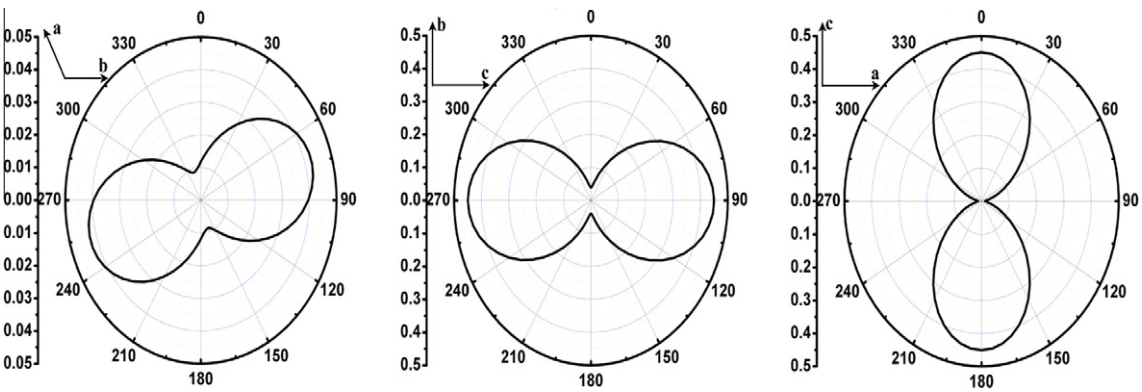

Fig. 6. Angular resolution anisotropic mobilities for hole transport in the *a*–*b*, *b*–*c* and *a*–*c* planes of the α-phase crystal structure.

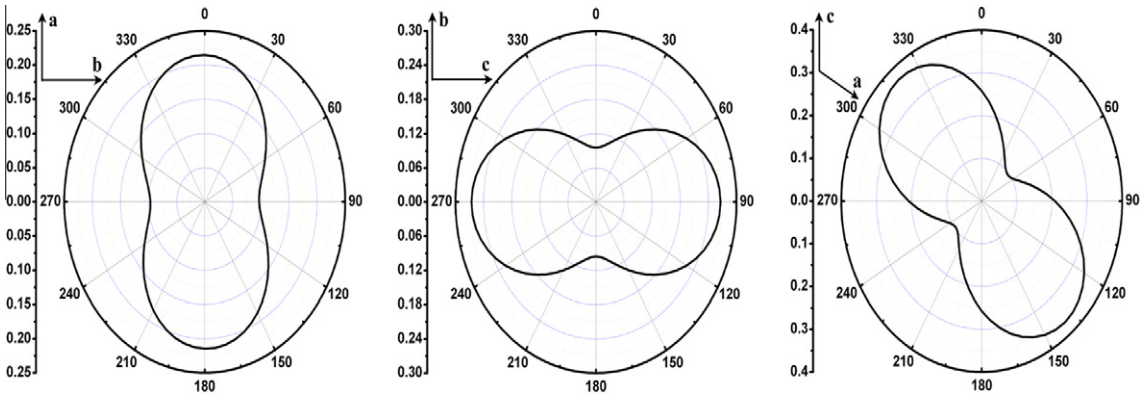

Fig. 7. Angular resolution anisotropic mobilities for hole transport in the *a*–*b*, *b*–*c* and *a*–*c* planes of the β-phase crystal structure.

4. Conclusion

The charge transport for DBTTF crystals in the α phase and β phase is investigated by employing the first-principles DFT calculations and the Marcus charge transfer theory. The random walk technique is developed to obtain the carrier mobilities for the 3D, 2D and 1D transport with a set of identical trajectories. It is found that the charge transport along the *c* axis plays a dominant role for the carrier mobilities in the α-phase crystal. This is attributed to that the π–π overlap between consecutive molecules along the *c* axis leads to strong electronic couplings which are much larger than those along the other pathways. For the β-phase crystal which presents the non-layered 3D stacks, the electronic couplings are more uniform in the 3D space, so the charge transport is relatively balanced along various directions although the mobility along any direction is smaller than that along the *c* axis of the α phase. Thus the 2D mobility of the β phase turns to be close to those of the α phase in the *b*–*c* and *a*–*c* planes and is obviously larger than that of the α phase in the *a*–*b* plane. As a result, the β-phase crystal presents a larger 3D mobility than the α-phase crystal. Since the charge transport in OFETs is mainly confined within the first few layers of the organic semiconductors/insulator interface [4,50,51] which corresponds to a quasi-3D structure for charge transport, the β-phase DBTTF crystal may have a larger potential for practical applications in organic electronics. At present, any measurement of carrier mobilities for the β-DBTTF has not been performed as far as we knows. Thus it is hoped that the present work can stimulate work in this direction.

Acknowledgements

This work is supported by the Major State Basic Research Development Programs of China (Grant No. 2011C BA00701), the National Natural Science Foundation of China (Grant Nos. 21003030 and 20973049) and the China Postdoctoral Science Foundation (Grant No. 20110490 102).

References

[1] H.E. Katz, Z.N. Bao, S.L. Gilat, Acc. Chem. Res. 34 (2001) 359.
[2] M.E. Gershenson, V. Podzorov, A.F. Morpurgo, Rev. Mod. Phys. 78 (2006) 973.
[3] J. Zaumseil, H. Sirringhaus, Chem. Rev. 107 (2007) 1296.
[4] C.D. Dimitrakopoulos, P.R.L. Malenfant, Adv. Mater. 14 (2002) 99.
[5] V.C. Sundar, J. Zaumseil, V. Podzorov, E. Menard, R.L. Willett, T. Someya, M.E. Gershenson, J.A. Rogers, Science 303 (2004) 1644.
[6] T. Sekitani, Y. Takamatsu, S. Nakano, T. Sakurai, T. Someya, Appl. Phys. Lett. 88 (2006) 253508.
[7] O.D. Jurchescu, M. Popinciuc, B.J. van Wees, T.T.M. Palstra, Adv. Mater. 19 (2007) 688.
[8] Y. Shirota, H. Kageyama, Chem. Rev. 107 (2007) 953.
[9] J.L. Segura, N. Martín, Angew. Chem. Int. Ed. 40 (2001) 1372.
[10] M. Mas-Torrent, C. Rovira, J. Mater. Chem. 16 (2006) 433.
[11] M. Mas-Torrent, M. Durkut, P. Hadley, X. Ribas, C. Rovira, J. Am. Chem. Soc. 126 (2004) 984.
[12] J. Naraso, S. Nishida, J. Ando, K. Yamaguchi, H. Itaka, H. Koinuma, S. Tada, Y. Tokito, Y. Yamashita, J. Am. Chem. Soc. 127 (2005) 10142.
[13] Y. Takahashi, T. Hasegawa, S. Horiuchi, R. Kumai, Y. Tokura, G. Saito, Chem. Mater. 19 (2007) 6382.
[14] M. Mas-Torrent, P. Hadley, S.T. Bromley, N. Crivillers, J. Veciana, C. Rovira, Appl. Phys. Lett. 86 (2005) 012110.
[15] T. Yamada, T. Hasegawa, M. Hiraoka, H. Matsui, Y. Tokura, G. Saito, Appl. Phys. Lett. 92 (2008) 233306.
[16] A. Brillante, I. Bilotti, R.G.D. Valle, E. Venuti, S. Milita, C. Dionigi, F. Borgatti, A.N. Lazar, F. Biscarini, M. Mas-Torrent, N.S. Oxtoby, N. Crivillers, J. Veciana, C. Rovira, M. Leufgen, G. Schmidt, L.W. Molenkamp, Cryst. Eng. Comm. 10 (2008) 1899.
[17] M. Mamada, Y. Yamashita, Acta Crystallogr., Sect. E 65 (2009) 2083.
[18] A.R. Murphy, J.M.J. Fréchet, Chem. Rev. 107 (2007) 1066.
[19] F. Würther, R. Schmidt, Chem. Phys. Chem. 7 (2006) 793.
[20] S. Schiefer, M. Huth, A. Dobrinevski, B. Nickel, J. Am. Chem. Soc. 129 (2007) 10316.
[21] G.R. Hutchison, M.A. Ratner, T.J. Marks, J. Am. Chem. Soc. 127 (2005) 2339.
[22] S. Mohakud, S.K. Pati, J. Mater. Chem. 19 (2009) 4356.
[23] W.Q. Deng, W.A. Goddard III, J. Phys. Chem. B 108 (2004) 8614.
[24] J.C. Sancho-García, A.J. Pérez-Jiménez, Y. Olivier, J. Cornil, Phys. Chem. Chem. Phys. 12 (2010) 9381.
[25] A. Troisi, G. Orlandi, J. Phys. Chem. A 110 (2006) 4065.
[26] L.J. Wang, Q.K. Li, Z.G. Shuai, L.P. Chen, Q. Shi, Phys. Chem. Chem. Phys. 12 (2010) 3309.
[27] Y.C. Cheng, R.J. Silbey, D.A. da Silva Filho, J.P. Calbert, J. Cornil, J.L. Brédas, J. Chem. Phys. 118 (2003) 3764.
[28] R.A. Marcus, Rev. Mod. Phys. 65 (1993) 599.
[29] J.E. Norton, J.L. Brédas, J. Am. Chem. Soc. 130 (2008) 12377.
[30] Y.A. Berlin, G.R. Hutchison, P. Rempala, M.A. Ratner, J. Michl, J. Phys. Chem. A 107 (2003) 3970.
[31] V. Coropceanu, M. Malagoli, D.A. da Silva Filho, N.E. Gruhn, T.G. Bill, J.L. Brédas, Phys. Rev. Lett. 89 (2002) 275503.
[32] M. Malagoli, J.L. Brédas, Chem. Phys. Lett. 327 (2000) 13.

[33] S.H. Wen, W.Q. Deng, K.L. Han, Phys. Chem. Chem. Phys. 12 (2010) 9267.
[34] V. Lemaur, D.A. da Silva Filho, V. Coropceanu, M. Lehmann, Y. Geerts, J. Piris, M.G. Debije, A.M. van de Craats, K. Senthilkumar, L.D.A. Siebbeles, J.M. Warman, J.L. Brédas, J. Cornil, J. Am. Chem. Soc. 126 (2004) 3271.
[35] J.R. Reimers, J. Chem. Phys. 115 (2001) 9103.
[36] M.J. Frisch, G.W. Trucks, H.B. Schlegel, G.E. Scuseria, M.A. Robb, J.R. Cheeseman, J.A. Montgomery, T. Vreven, K.N. Kudin, J.C. Burant, J.M. Millam, S.S. Iyengar, J. Tomasi, V. Barone, B. Mennucci, M. Cossi, G. Scalmani, N. Rega, G.A. Petersson, H. Nakatsuji, M. Hada, M. Ehara, K. Toyota, R. Fukuda, J. Hasegawa, M. Ishida, T. Nakajima, Y. Honda, O. Kitao, H. Nakai, M. Klene, X. Li, J.E. Knox, H.P. Hratchian, J.B. Cross, V. Bakken, C. Adamo, J. Jaramillo, R. Gomperts, R.E. Stratmann, O. Yazyev, A.J. Austin, R. Cammi, C. Pomelli, J.W. Ochterski, P.Y. Ayala, K. Morokuma, G.A. Voth, P. Salvador, J.J. Dannenberg, V.G. Zakrzewski, S. Dapprich, A.D. Daniels, M.C. Strain, O. Farkas, D.K. Malick, A.D. Rabuck, K. Raghavachari, J.B. Foresman, J.V. Ortiz, Q. Cui, A.G. Baboul, S. Clifford, J. Cioslowski, B.B. Stefanov, G. Liu, A. Liashenko, P. Piskorz, I. Komaromi, R.L. Martin, D.J. Fox, T. Keith, M.A. Al-Laham, C.Y. Peng, A. Nanayakkara, M. Challacombe, P.M.W. Gill, B. Johnson, W. Chen, M.W. Wong, C. Gonzalez, J.A. Pople, Gaussian 03 (Revision E01), Gaussian, Inc., Wallingford CT, 2004.
[37] J.L. Brédas, D. Beljonne, V. Coropceanu, J. Cornil, Chem. Rev. 104 (2004) 4971.
[38] J.S. Huang, M. Kertesz, J. Chem. Phys. 122 (2005) 234707.
[39] A. Troisi, G. Orlandi, Chem. Phys. Lett. 344 (2001) 509.
[40] G.J. Nan, X.D. Yang, L.J. Wang, Z.G. Shuai, Y. Zhao, Phys. Rev. B 79 (2009) 115203.
[41] S.W. Yin, Y.P. Yi, Q.X. Li, G. Yu, Y.Q. Liu, Z.G. Shuai, J. Phys. Chem. A 110 (2006) 7138.
[42] G.R. Hutchison, M.A. Ratner, T.J. Marks, J. Am. Chem. Soc. 127 (2005) 16866.
[43] J.L. Brédas, J.P. Calbert, D.A. da Silva Filho, J. Cornil, Proc. Natl. Acad. Sci. USA 99 (2002) 5804.
[44] X.Y. Li, J. Comput. Chem. 22 (2001) 565.
[45] E.F. Valeev, V. Coropceanu, D.A. da Silva Filho, S. Salman, J.L. Brédas, J. Am. Chem. Soc. 128 (2006) 9882.
[46] K. Senthilkumar, F.C. Grozema, F.M. Bickelhaupt, L.D.A. Siebbeles, J. Chem. Phys. 119 (2003) 9809.
[47] G.J. Nan, L.J. Wang, X.D. Yang, Z.G. Shuai, Y. Zhao, J. Chem. Phys. 130 (2009) 024704.
[48] V. Coropceanu, J. Cornil, D.A. da Silva Filho, Y. Olivier, R. Silbey, J.L. Brédas, Chem. Rev. 107 (2007) 926.
[49] L.J. Wang, G.J. Nan, X.D. Yang, Q. Peng, Q.K. Li, Z.G. Shuai, Chem. Soc. Rev. 39 (2010) 423.
[50] F. Dinelli, M. Murgia, P. Levy, M. Cavallini, F. Biscarini, Phys. Rev. Lett. 92 (2004) 116802.
[51] A. Dodabalapur, L. Torsi, H.E. Katz, Science 268 (1995) 270.
[52] G.J. Nan, Q. Shi, Z.G. Shuai, Z.S. Li, Phys. Chem. Chem. Phys. 13 (2011) 9736.
[53] G.J. Nan, Z.S. Li, Comput. Theor. Chem. (2012) submitted.
[54] V. Podzorov, E. Menard, A. Borissov, V. Kiryukhin, J.A. Rogers, M.E. Gershenson, Phys. Rev. Lett. 93 (2004) 086602.
[55] C. Reese, Z.N. Bao, Adv. Mater. 19 (2007) 4535.
[56] J.Y. Lee, S. Roth, Y.W. Park, Appl. Phys. Lett. 88 (2006) 252106.
[57] It should be mentioned that the waiting time is often featured with a random number in disordered organic materials. For example, the waiting time τ is calculated as $\tau = -\frac{1}{\Gamma}\log\gamma$ in Ref. [58] where γ is a random number with the uniform distribution in [0,1] and Γ is the total hopping rate for the site where the carrier is located at the moment. Then the waiting time varies for each hopping which results from the different dwelling environment for carrier in disordered systems. For the present case, however, the carrier can always feel the same dwelling environment wherever it is located, so the waiting time should not alter when the hopping occurs. In fact, the waiting time in this work is calculated as $\tau = -\frac{1}{\Gamma}\log\gamma$ with $\gamma = 0.1$ for brevity. When different random numbers are used for waiting time, the carrier mobilities are proportionally increased or decreased at the same time for the α- and β-phase crystal structures of DBTTF, which thus has not any influence for the conclusion made in this work.
[58] S.V. Novikov, Phys. Stat. Sol. (c) 5 (2008) 740.
[59] O. Kwon, V. Coropceanu, N.E. Gruhn, J.C. Durivage, J.G. Laquindanum, H.E. Katz, J. Cornil, J.L. Brédas, J. Chem. Phys. 120 (2004) 8186.
[60] H. Kojima, T. Mori, Bull. Chem. Soc. Jpn. 84 (2011) 1049.
[61] J. Nagakubo, M. Ashizawa, T. Kawamoto, A. Tanioka, T. Mori, Phys. Chem. Chem. Phys. 13 (2011) 14370.